2007

Aerosol Properties Computed from Aircraft-Based Observations During the ACE-Asia Campaign: 2. A Case Study of Lidar Ratio Closure

M. Kuzmanoski
University of New South Wales, mkuzm@phys.unsw.edu.au

M. A. Box
University of New South Wales

B. Schmid
Bay Area Environmental Research Institute, Sonoma, California, USA

G. P. Box
University of New South Wales

J. Wang
Brookhaven National Laboratory, Upton, New York, USA

See next page for additional authors

Aerosol Science and Technology, 41:231–243, 2007

ISSN: 0278-6826 print / 1521-7388 online
DOI: 10.1080/02786820601146977

Aerosol Properties Computed from Aircraft-Based Observations During the ACE-Asia Campaign: 2. A Case Study of Lidar Ratio Closure

M. Kuzmanoski,[1,2] M. A. Box,[1] B. Schmid,[2,3] G. P. Box,[1] J. Wang,[4] P. B. Russell,[5] D. Bates,[6] H. H. Jonsson,[7] E. J. Welton,[8] and J. H. Seinfeld[9]

[1]*School of Physics, University of New South Wales, Sydney, Australia*
[2]*Bay Area Environmental Research Institute, Sonoma, California, USA*
[3]*Now at Pacific Northwest National Laboratory, Richland, Washington, USA*
[4]*Brookhaven National Laboratory, Upton, New York, USA*
[5]*NASA Ames Research Center, Moffett Field, California, USA*
[6]*Physics Department, University of Miami, Coral Gables, Florida, USA*
[7]*CIRPAS, Marina, California, USA*
[8]*NASA Goddard Space Flight Center, Laboratory for Atmospheres, Greenbelt, Maryland, USA*
[9]*Department of Chemical Engineering, California Institute of Technology, Pasadena, California, USA*

For a vertical profile with three distinct layers (marine boundary, pollution, and dust layers), observed during the ACE-Asia campaign, we carried out a comparison between the modeled lidar ratio vertical profile and that obtained from co-located airborne NASA AATS-14 sunphotometer and shipborne Micro-Pulse Lidar (MPL) measurements. The vertically resolved lidar ratio was calculated from two size distribution vertical profiles—one obtained by inversion of sunphotometer-derived extinction spectra, and one measured in-situ—combined with the same refractive index model based on aerosol chemical composition. The aerosol model implies single scattering albedos of 0.78–0.81 and 0.93–0.96 at 0.523 μm (the wavelength of the lidar measurements), in the pollution and dust layers, respectively. The lidar ratios calculated from the two size distribution profiles agree closely in the dust layer; they are however, significantly lower than the lidar ratios derived from combined lidar and sunphotometer measurements. Uncertainties in aerosol size distributions and refractive index only partly explain these differences, suggesting that particle nonsphericity in this layer is an additional explanation. In the pollution layer, the two size distribution profiles yield lidar ratios that agree within the estimated uncertainties. The retrieved size distributions result in a lidar ratio which is in closer agreement with that derived from lidar/sunphotometer measurements in this layer, with still large differences at certain altitudes (the largest relative difference was 46%). We explain these differences by non-uniqueness of the result of the size distribution retrieval, by a lack of information on the mixing state of particles, and the vertical variability of the particle refractive index.

Received 20 February 2006; accepted 30 November 2006.

This work was carried out while one author (M. K.) was supported by an International Postgraduate Research Scholarship, funded by the Australian Department of Education, Science and Training (DEST). MPLNET is funded by the NASA Earth Observing System and Radiation Sciences Program. We would like to thank Jens Redemann for his detailed review of an earlier version of the manuscript and helpful comments. We would also like to thank the anonymous reviewers for their valuable comments and suggestions.

Address correspondence to M. Kuzmanoski, School of Physics, University of New South Wales, Sydney, NSW 2052, Australia. E-mail: mkuzm@phys.unsw.edu.au

1. INTRODUCTION

Radiative forcing caused by aerosols is one of the major uncertainties in estimating the Earth's radiation budget (Intergovernmental Panel on Climate Change (IPCC), 2001). The impact of aerosols on climate is controlled by aerosol optical properties, such as optical thickness, single scattering albedo and asymmetry parameter. These quantities can be derived from measurements, or evaluated from the available information on aerosol size distribution, shape, chemical composition and mixing state. Comparative studies of different measurement methods, as well as measured and modeled aerosol optical properties, are useful in efforts to improve our understanding of the role of aerosols in radiative transfer. Such studies are referred to as closure studies, and are one of major focuses of the ACE-Asia campaign (Huebert et al. 2003) and previous aerosol characterization experiments, such as ACE 1 (Bates et al. 1998), ACE 2 (Russell and Heintzenberg 2000), TARFOX (Russell et al. 1999), and LACE 98 (Ansmann et al. 2002).

The lidar ratio, or extinction-to-backscatter ratio, is an essential parameter for retrieving quantitative aerosol information from backscatter lidars. While independent measurements of

extinction and backscattering coefficient vertical profiles can be obtained by Raman lidar (Ansmann et al. 1990, 1992) and high-spectral resolution lidar (Shipley et al. 1983; Grund and Eloranta 1990), obtaining the extinction coefficient from elastic backscatter lidar measurements requires a priori knowledge of the lidar ratio. This property can be obtained by combining backscatter lidar measurements with information on layer optical thickness, derived from coincident radiometer or sunphotometer measurements (Welton et al. 2000), or from slant-path lidar measurements (Spinhirne et al. 1980; Powell et al. 2000). McGill et al. (2003) employed the transmission loss method to determine the lidar ratio of a cloud or an elevated aerosol layer located between two clean layers directly from Cloud Physics Lidar data. Schmid et al. (2003) combined airborne sunphotometer and shipborne lidar measurements to derive the vertical profile of the lidar ratio needed to yield close agreement between the lidar-derived and sunphotometer-derived vertical profiles of aerosol extinction. The lidar ratio can also be estimated from aerosol size distributions (measured in-situ, or retrieved from aerosol optical properties) and a suitable refractive index model.

In the present work, a comparison of the modeled vertical profile of lidar ratio, with the one derived by Schmid et al. (2003) from co-located airborne sunphotometer and shipborne lidar measurements (the implied lidar ratio), is carried out. Previous studies on comparisons of lidar measurements with calculations from in-situ measured size distributions concentrated mainly on minimizing the differences between the modeled and measured extinction and backscattering, in order to find the real part of the refractive index and the single scattering albedo (Redemann et al. 1998, 2000; Ferrare et al. 1998), or used information on aerosol chemical composition in order to derive the mixing state (Fiebig et al. 2002). Some studies focused on comparison of directly measured lidar ratio and that derived from aerosol size distributions, using Mie theory (Liu et al. 2002; Masonis et al. 2003). The lidar ratio can also be predicted from information on wavelength dependence of aerosol extinction, using aerosol size distribution retrieval as an intermediate step. Rajeev and Parameswaran (1998) employed the size distribution retrieval method of King et al. (1978) in an iterative algorithm for analyzing multi-wavelength lidar signal to obtain vertical profiles of aerosol extinction spectra and size distributions. They derived vertical profiles of extinction spectra from lidar measurements, using an assumed lidar ratio; in the next iteration they used a new lidar ratio estimate calculated from the size distributions retrieved from the extinction spectra. A similar approach, which involves size distribution retrieval, is used here as a means of comparing airborne sunphotometer with lidar measurements. We compare lidar ratios modeled using size distributions retrieved from sunphotometer-derived aerosol extinction spectra, with those obtained from combined sunphotometer and lidar measurements.

Focusing on the aerosol profile observed on April 17, 2001 as part of the ACE-Asia campaign, and studied in Part I for aerosol size distributions (Kuzmanoski et al. 2006), we compare lidar ratios calculated from two size distribution profiles—one retrieved from sunphotometer-derived extinction, and one measured in-situ—in three distinct layers observed on this day. The refractive index model used is based on the analysis of aerosol chemical composition. Modeled lidar ratios are compared with the one derived from co-located airborne sunphotometer and shipbased backscatter lidar measurements. While aerosol extinction is sensitive mainly to aerosol size distribution and the real part of the refractive index, lidar ratio also shows sensitivity to the imaginary part of the refractive index, mixing state, and shape of the particles, because of the dependence of the backscattering coefficient on these particle properties. Thus, comparison of modeled and measured values of lidar ratio is convenient for testing the validity of the aerosol model for use in estimating other aerosol properties.

2. MEASUREMENTS

Measurements relevant for this work were carried out aboard the CIRPAS Twin Otter aircraft (Bane et al. 2004). The details about aerosol optical depth and size distribution measurements are given by Schmid et al. (2003) and Wang et al. (2002), respectively. In brief, aerosol optical depth was measured at 13 wavelengths, in the wavelength range from 0.354 μm to 1.558 μm, using the 14-channel NASA Ames Airborne Sun-tracking Sunphotometer (AATS-14). Schmid et al. (2003) differentiated aerosol optical depths measured in vertical profiles to obtain aerosol extinction. In the present work, the aerosol extinction spectra are used for the retrieval of the vertical profile of aerosol size distribution. At the same time size distribution measurements were made using a combination of a Differential Mobility Analyzer (DMA) System, for measurements in the 0.015–1.0 μm particle diameter range, and an Aerodynamic Particle Sizer (APS) for the 0.5–10 μm diameter range (Wang et al. 2002).

For aerosol chemical composition measurements, 8 Micro-Orifice Uniform Deposit Impactors (MOUDI) and 3 denuder samplers operated aboard the Twin Otter aircraft (Wang et al. 2002). Although each MOUDI had 5 stages, only one of them (collecting particles with diameters up to 3 μm) was in operation. The collected samples were analyzed for metallic elements, and water-soluble anionic species, while the denuder samplers were used for analyzing organic carbon (OC) and elemental carbon (EC). A Tandem DMA was used for measurement of aerosol hygroscopic properties.

The Micro-Pulse Lidar (MPL) (Spinhirne et al. 1995) is an eye-safe single channel backscatter lidar at 0.523 μm. NASA operates a network of these instruments called MPLNET (Welton et al. 2001), co-located with AERONET sun/sky photometers (Holben et al. 1998). During ACE-Asia, MPL measurements were conducted aboard the NOAA ship R/V Ronald H. Brown to determine the vertical profile of aerosol extinction. Analysis of backscatter lidar data requires knowledge of the

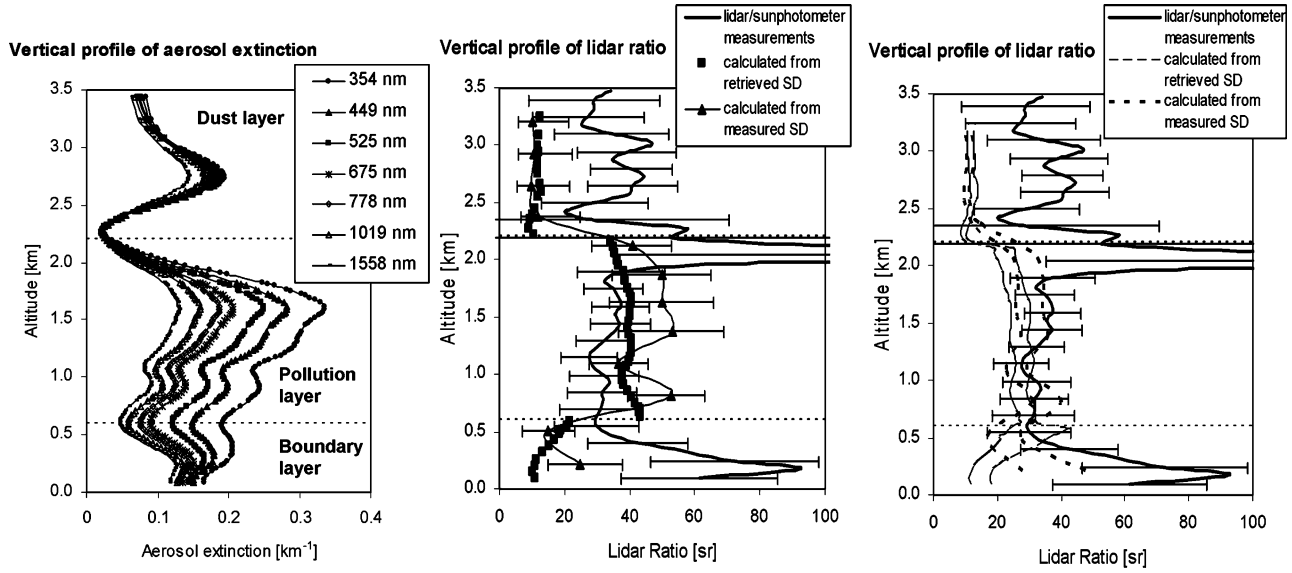

FIG. 1. **(left)** Vertical profile of aerosol extinction at different wavelengths, derived from sunphotometer measurements on April 17 (Schmid et al. 2003). **(middle)** Vertical profiles of the lidar ratio derived from sunphotometer/lidar measurements (implied lidar ratio) (Schmid et al. 2003), and the lidar ratios calculated from the retrieved and in-situ measured size distributions. The error bars in the lidar ratios modeled from the measured size distributions are due to uncertainties in size distributions and real part of refractive index. **(right)** The lidar ratio modeled profiles which correspond to single scattering albedo values of 0.88 and 0.98 in the boundary layer, 0.88 and 0.94 in the pollution layer, and 0.92 and 0.96 in the dust layer.

extinction-to-backscatter ratio (lidar ratio) to generate extinction profiles. MPLNET standard procedure uses column aerosol optical depth from co-located ground-based photometers to constrain the lidar solution and calculate a layer averaged lidar ratio.

Three Twin Otter vertical profiles during the ACE-Asia campaign coincided with the lidar measurements aboard the R/V Ronald H. Brown. Schmid et al. (2003) utilized a modified lidar solution to obtain a vertical profile of the lidar ratio using the aerosol optical depth profile from AATS-14. They call this profile the implied lidar ratio. Here we calculate two new lidar ratio profiles using both the in-situ measured, and AATS-14 retrieved, size distributions and compare them to the implied lidar ratio profile. We concentrate on the April 17, 2001 profile for which we are able to derive the aerosol refractive index values from the airborne chemical measurements. On this day, the aircraft flew a vertical profile from 0.09 to 3.43 km, south of Jeju island, Korea, near the coast (33°N, 128°E). The left panel of Figure 1 shows the extinction profile derived by Schmid et al. (2003) from the sunphotometer measurements, and boundaries between three distinct layers observed: marine boundary, pollution, and dust layer, all with different particle physical and chemical characteristics. The backtrajectory analysis showed that the pollution layer originated from mainland China (Wang et al. 2002).

The formula used in this paper for calculation of the lidar ratio is:

$$S = \frac{4\pi}{\omega_0 \cdot p(180^\circ)}. \qquad [1]$$

Here, ω_0 is the single scattering albedo, and $p(180^\circ)$ is the phase function in the backscattering direction, with normalization:

$$\frac{1}{2}\int_0^\pi p(\theta)\sin\theta d\theta = 1 \qquad [2]$$

3. AEROSOL MODEL

As noted previously, we obtained the size distribution vertical profiles from the in-situ measurements, using DMA and APS, and by inversion of sunphotometer-derived extinction spectra. DMA and APS measured size distributions in the particle diameter range 0.015–10.0 μm, at several altitudes within each layer. Uncertainties in the measured size distributions, in different size ranges, are given in Table 1. The data used here were adjusted to ambient relative humidity (RH). In-situ measurements of size distributions at particle diameters $D_p < 0.5$ μm

TABLE 1
Uncertainties in in-situ measured aerosol size distributions (Wang et al. 2002) (note that these uncertainties do not include uncertainties associated with adjustment to ambient RH)

Particle diameter range	Uncertainty in particle size measurements	Uncertainty in concentration measurements
$D_p < 0.5$ μm	±5%	±10%
0.5 μm < D_p < 5000 nm	±10%	±20%
D_p >5000 nm	±10%	±50%

were carried out using a DMA system. The RH inside the DMA was maintained the same as the ambient RH, by adding the appropriate amount of water vapor to compensate for ram heating. The uncertainty associated with the adjustment to ambient RH is negligible in the particle size range of DMA measurements. For larger particle sizes, at which the measurements were taken using an APS, the adjustment to ambient RH was calculated by Wang et al. (2002) using the measured chemical composition and differences between APS RH and ambient RH.

The size distribution retrievals from measured extinction spectra were carried out with a vertical resolution of ~40–50 m, using the constrained linear inversion method (King et al. 1978). Because of the non-uniqueness of the retrieved size distributions (King et al. 1978, 1982), instead of estimating their uncertainties, we carried out analysis similar to that reported by Gonzalez Jorge and Ogren (1996) to estimate the quality of modeled optical properties based on these size distributions; for that purpose we compared the optical properties calculated from the size distributions used for generating extinction spectra, and the corresponding properties calculated from size distributions retrieved from the generated extinctions. The details of this analysis are described later in this section.

Both the retrieved and measured size distribution profiles were combined with the size-resolved refractive index (calculated by Wang et al. 2002) based on aerosol chemical composition measured in each layer, to calculate the single scattering albedo and backscattering phase function. The chemical composition measurements in the boundary, pollution, and dust layers were taken at the altitudes of 0.04, 1.38, and 2.81 km, respectively. Wang et al. (2002) calculated the size-resolved refractive index, assuming that the fine mode consisted of SO_4^{2-}, NO_3^-, NH_4^+, OC, and EC, while the coarse mode consisted of sea salt and dust (this assumption was based on reported observations). The details of determining the size boundary between the two modes are discussed by Wang et al. (2002). They calculated the refractive index values for each of the layers observed in the profile, assuming that aerosols were internal mixtures of different species, and using the Bruggeman mixing rule (Bruggeman 1935). The assumption of an internal mixture was justified by the results of the Tandem DMA measurements, which revealed that particles of the same dry size grew to similar sizes at high RH. At a fixed RH value, the water uptake and aqueous phase composition were calculated using ISSOROPIA (a thermodynamic equilibrium model for multiphase multicomponent inorganic aerosol) (Nenes et al. 1998), which uses the concentrations of SO_4^{2-}, NO_3^-, NH_4^+, Na^+, and Cl^- as inputs. Since there was no information on vertical variation of the refractive index, one value was used here at all altitudes within each layer. While the coarse mode particles in the boundary and dust layers were dominated by one component (sea salt or dust), in the pollution layer they were mixtures of the two components (with the dust/sea salt mass fractions ~30%/70%) (Wang et al. 2002). Since the external mixture of dust and sea salt in the coarse mode is more realistic than the internal mixture which was assumed in the size-resolved refractive index model used here, the effect of particle mixing state on calculated optical properties will be discussed in Sections 4 and 5.

It should be noted that the size distribution retrievals were carried out using a constant refractive index (not dependent on particle size and wavelength), since this is how the inversion code is set up. As shown in Part I, and also discussed by King et al. (1978) and Gonzalez Jorge and Ogren (1996), this assumption affects the resulting size distributions. This leads to the conclusion that the retrieved size distributions, combined with the size-resolved refractive index, do not necessarily reproduce the spectral shape of the measured extinction. In order to create an aerosol model consistent with the sunphotometer measurements, the size distribution retrievals were repeated for several different refractive index values, chosen from the range of values at different particle sizes. In this way, the size distribution result which, along with the size resolved refractive index, reproduces well the measured spectral dependence of the extinction, was found.

In order to estimate the uncertainties in optical properties modeled from the retrieved size distributions, we generated aerosol extinction spectra in the AATS-14 spectral range (0.354–1.558 μm) using bimodal lognormal size distributions with modal radii (for surface area size distributions) of 0.08, 0.10, and 0.12 μm for the fine mode, and 0.8, 1.0, and 1.2 μm for the coarse mode, and modal widths 0.50 and 0.70 for these two modes respectively. For each combination of fine and coarse modes, their ratio was adjusted to obtain different wavelength dependencies of aerosol extinction, similar to those obtained from sunphotometer measurements in the studied case. The dependencies were given by Ångström exponent values α (where $\tau_{\text{ext}} \sim \lambda^{-\alpha}$) of 0.1, 0.6, and 0.9. Using the constrained linear inversion method, we retrieved size distributions (for different particle radius ranges) from the generated extinction spectra, and we calculated aerosol single scattering albedo and lidar ratio from these size distributions. In this analysis, the refractive index was assumed to be known, and the same for the two modes. For a limited set of parameters (modal radii and Ångström exponents) typical for the pollution layer in this study, we repeated the analysis using the assumption of different refractive indices for the two modes.

As shown by Wang et al. (2002) and Kuzmanoski et al. (2006), the two size distribution models yield similar spectral dependencies of the aerosol extinction in the pollution and dust layers. However, comparison of retrieved and layer-averaged measured size distributions in these layers (Figures 2 and 3) suggest that the retrieved distributions have larger concentrations at both small and large particle ends in comparison with the measured size distributions. Results of retrievals from layer optical thicknesses (divided by the geometrical thickness of the layer) are presented, rather than average size distributions retrieved from aerosol extinctions, as they are better constrained due to less uncertainty in optical thickness than in extinction. In the lower part of the boundary layer (at about 0.2 km), the

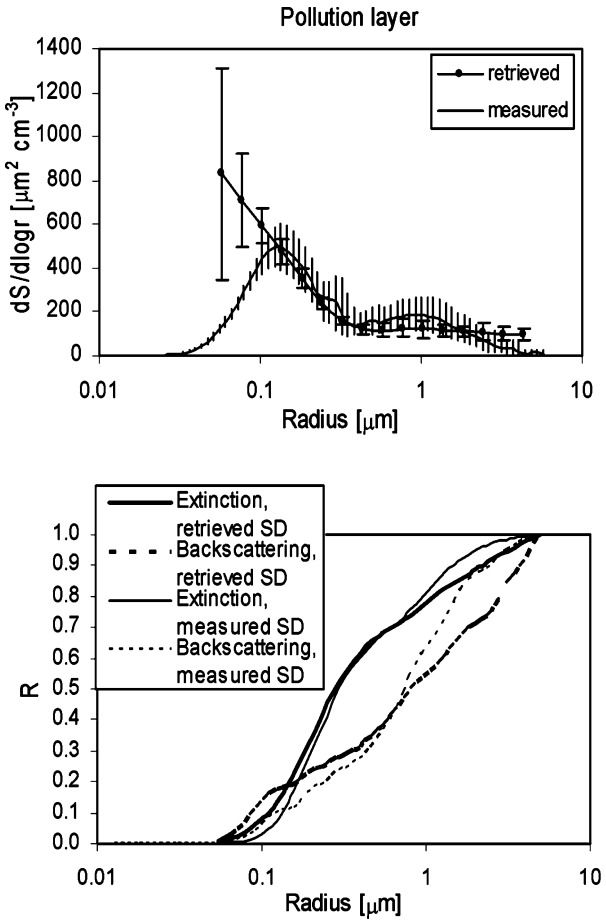

FIG. 2. **(top)** Comparison of size distribution retrieved from the sunphotometer-derived aerosol layer optical thickness spectrum, with the layer-averaged in-situ measured size distribution in the pollution layer (Kuzmanoski et al. 2006). **(bottom)** Corresponding extinction and backscattering contribution functions R.

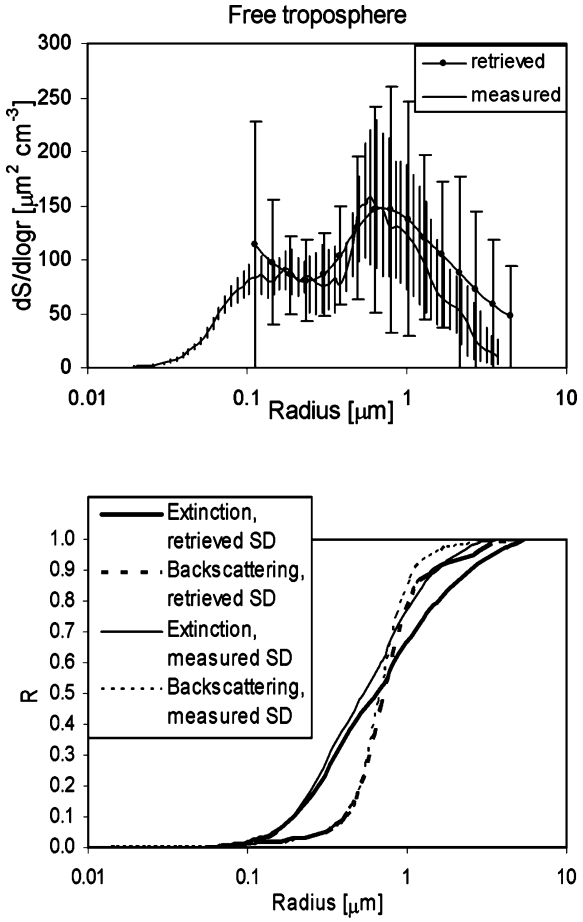

FIG. 3. **(top)** Comparison of size distribution retrieved from the sunphotometer-derived layer aerosol optical thickness spectrum, with the layer-averaged in-situ measured size distribution in the dust layer (Kuzmanoski et al. 2006). **(bottom)** Corresponding extinction and backscattering contribution functions.

measured size distribution showed larger relative concentration of fine mode particles than the size distributions retrieved from the sunphotometer-derived aerosol extinction; this is consistent with a stronger wavelength dependence of extinction calculated from the measured size distribution, in comparison with those derived from sunphotometer measurements at similar altitudes. Wang et al. (2002) explained this by layer inhomogeneity (the extinction is derived from the sunphotometer measurements using an assumption that the sunphotometer-to-sun path passes through horizontally homogeneous layers). These differences are, however, less pronounced in the upper part of the boundary layer. The effect of the differences between the measured and retrieved size distributions on corresponding modeled aerosol optical properties (single scattering albedo and lidar ratio) are discussed in Section 4.

4. AEROSOL OPTICAL PROPERTIES

The calculation of aerosol single scattering albedo and backscattering phase function was carried out using Mishchenko's Mie code (Mishchenko et al. 1999; De Rooij and Van der Stap 1984). Due to irregular shapes of dust particles (Sokolik et al. 2001; Kalashnikova and Sokolik 2002, 2004), the assumption of spherical particles in the dust layer may result in erroneous modeled optical properties. Studies that investigated the effect of this assumption on various calculated aerosol properties (Mishchenko et al. 1997; Pilinis and Li 1998) show that the optical thickness and single scattering albedo are not significantly affected by the particle nonsphericity, while the backscattering phase function at 180° is overestimated by use of Mie theory in the case of nonspherical particles. The effect of particle nonsphericity on modeled lidar ratio will be discussed in Section 5.

4.1. Single Scattering Albedo

Both size distribution models (measured in-situ, and retrieved from sunphotometer measurements) yield similar single scattering albedo values, with not much vertical variability within each layer, as a result of its stronger dependence on the

refractive index than its dependence on the particle size. The chemical composition analysis implied nonabsorbing particles in the boundary layer (Wang et al. 2002), which resulted in single scattering albedo values equal to 1.0. Single scattering albedo values of 0.78–0.81 ($\lambda = 0.523$ μm) in the pollution layer, and 0.93–0.96 in the dust layer, were found from both size distribution profiles, as particles in these two layers were absorbing due to the presence of elemental carbon in the accumulation mode, and dust in the coarse mode, respectively (Wang et al. 2002). The largest difference between the single scattering albedo values resulting from the two size distribution models is $\sim$0.02 in these layers. The assumption of an external mixture of sea salt and dust in the coarse mode was found to have negligible effect on the modeled single scattering albedo. The modeled single scattering albedo is not very sensitive to expected variations in aerosol size distribution and the real part of the refractive index (variations in single scattering albedo obtained in our analysis were smaller than 0.02): it depends mainly on the imaginary part of aerosol refractive index. The modeled single scattering albedo in the pollution layer is significantly lower than the values obtained from airborne and shipborne measurements in polluted airmasses observed during the campaign, and reported in several other studies. The average single scattering albedo of the submicron particle mode in the pollution layers, obtained from the in-situ measurements of particle scattering and absorption aboard the NCAR C-130 aircraft during the ACE-Asia campaign, was 0.88 $\pm$ 0.03 at 0.55 μm, at RH below 40% (Anderson et al. 2003). Bergstrom et al. (2003) determined wavelength-dependent single scattering albedo which reproduces aerosol layer fractional absorption derived from Solar Spectral Flux Radiometer (SSFR) measurements aboard the Twin Otter aircraft. For a layer influenced by pollution and dust, observed on April 12, 2001, they reported a single scattering albedo value of 0.90 $\pm$ 0.02 at 0.55 μm, with stronger wavelength dependence than that of the single scattering albedo calculated here for the pollution layer. Quinn et al. (2004) obtained single scattering albedo values of 0.90–0.94 for polluted regions at 55% RH, from in-situ measurements aboard the R/V Ronald H. Brown during the ACE-Asia campaign. Markowicz et al. (2003) reported single scattering albedos above 0.86 at 55% RH for polluted airmasses. Carrico et al. (2003) obtained the single scattering albedo as a function of RH: they used the humidograph nephelometer method to determine dependence of aerosol scattering coefficient on RH, and PSAP measurements of absorption coefficient at 55% RH, and assumed that the change of absorption coefficient with RH is negligible. Their results showed that in the polluted regions during the campaign the single scattering albedo increased from 0.91 to 0.96 for an increase in RH from 40% to 85%. They also reported an average single scattering albedo of 0.94 $\pm$ 0.03 at ambient RH (71 $\pm$ 13%). While bearing in mind that a single, highly polluted, aerosol profile is studied here, and it could therefore display smaller single scattering albedo than average values during the campaign, it is useful to discuss other possible reasons for these differences. Our analysis showed that lower values of imaginary part of the refractive index, that would result in single scattering albedo in agreement with the measurements described above (0.88–0.94), could be explained by uncertainty in EC refractive index values found in the literature: Wang et al. (2002) used the EC refractive index value of 1.9 + 0.66 i, while a lower value of 1.74 + 0.45 i was reported in the OPAC database (Hess et al. 1998). However, it should also be noted that the large difference between our modeled value of single scattering albedo and the values reported in the literature could be a result of layer inhomogeneity, reported by Wang et al. (2002): the aerosol model used here is based on aerosol chemical composition measured at a single altitude, and could therefore be non-representative for the entire pollution layer.

The modeled single scattering albedo for the dust layer in the present work (0.93–0.96 at $\lambda = 0.523$ μm) is in agreement with shipborne and airborne in-situ measurements for dust cases: Quinn et al. (2004) and Carrico et al. (2003) reported the average single scattering albedo value of 0.94 $\pm$ 0.02 in dust airmasses during ACE-Asia, and Anderson et al. (2003) reported 0.96 $\pm$ 0.01 for coarse mode dust particles.

The modeled single scattering albedo in the boundary layer is at the upper limit of the values reported by Quinn et al. (2004) (0.99 $\pm$ 0.01) for maritime aerosol at ambient RH. Note however that this layer was also reported to be inhomogeneous (Wang et al. 2002) and that there is no clear distinction between the boundary and pollution layers in this profile: consequently, application of one refractive index model in the entire layer could result in incorrect modeled single scattering albedo. This possibility will be further discussed in the Section 5.

4.2. Modeled Lidar Ratio

Vertically resolved lidar ratios modeled using the measured and retrieved size distributions exhibit differences in the pollution and the lower part of the boundary layer, but agree well in the dust layer and the upper part of the boundary layer (Figure 1). The discontinuities in the modeled lidar ratio profile at the boundaries between the layers are a result of the change of refractive index used in the calculations, and suggest that there is a variability in this aerosol property with altitude within each layer.

It is important to note that the very low lidar ratio values in the dust layer are a result of the assumption of spherical particles, used in the aerosol model, while low values in the boundary layer are attributed to the layer inhomogeneity and uncertainties in refractive index used in the model. Both these effects will be discussed in more detail in Section 5. The lidar ratio values calculated from the measured size distributions in the pollution layer exhibit more vertical variability and generally larger values than those resulting from the retrieved size distributions. The average calculated lidar ratio values in the studied layers are given in Table 2. Since the same refractive index values were used in both models for calculation of the lidar

TABLE 2
Aerosol size-dependent refractive indices based on aerosol chemical analysis (Wang et al. 2002), in three layers observed in the vertical profile of April 17, and average lidar ratio values calculated from retrieved and measured size distributions.

	Refractive index		Modeled lidar ratio (sr)	
Aerosol layer	Real part	Imaginary part	Retrieved SD	Measured SD
Dust layer	1.51–1.56	0–0.003	11.9 (6.1–24.8)*	10.4 (6.0–21.9)*
Pollution layer	1.40–1.54	0.0003–0.046	39.5 (22.1–50.6)*	48.1 (22.4–61.2)*
Boundary layer	1.53–1.54	0	14.1 (7.3–28.2)*	17.3 (7.6–17.2)*

*The range of values within the estimated uncertainties.

ratio, the different lidar ratios are a result of size distribution differences.

In the lower part of the boundary layer, larger lidar ratio calculated from the measured size distribution compared to those resulting from the retrieved size distributions is consistent with the larger relative concentration of fine mode particles, discussed earlier. As noted by Liu et al. (2002), an increase in the relative concentration of fine mode particles results in increased lidar ratios. The difference between the size distributions could be explained by inhomogeneity of this aerosol layer, which affects sunphotometer-derived extinction (Wang et al. 2002). In the upper part of the layer, however, the difference between the modeled lidar ratios is significantly smaller, and can be explained by size distribution uncertainties.

For better understanding of the effect of the differences in the size distributions on the computed lidar ratio values in the pollution and dust layers, the relative contributions of particles in different size ranges to extinction and backscattering coefficients were calculated following Russell et al. (1981) and Reagan et al. (1988):

$$R_{\mathrm{ext,bsc}}(\tilde{r}) = \frac{\int_{r_1}^{\tilde{r}} \pi r^2 Q_{\mathrm{ext,bsc}}(r, \lambda, m) dr}{\int_{r_1}^{r_2} \pi r^2 Q_{\mathrm{ext,bsc}}(r, \lambda, m) dr} \quad [3]$$

$R_{\mathrm{ext,bsc}}(\tilde{r})$ is the relative contribution of the particles with radii smaller than $\tilde{r}$, to the extinction or backscattering due to all particles between lower and upper radius limits (r_1 and r_2) of the given size distribution. The relative contributions calculated at $\lambda = 0.523$ μm for aerosol size distributions (layer-averaged in-situ measured, and retrieved from layer optical thickness spectra) in these two layers are shown in Figures 2 and 3.

Examining the differences between the retrieved and measured size distributions in the pollution layer, in parallel with the corresponding contribution factors, reveals the following major reason for the generally smaller lidar ratio resulting from the retrieved size distributions. As noted earlier, in comparison with the measured size distributions, the retrieved distributions have larger concentrations at both small and large particle ends. The contribution of these particles to the backscattering coefficient is generally larger than their contribution to extinction, particularly at the large particle end, leading to a smaller lidar ratio. The contribution factors shown in Figure 2 suggest that in the pollution layer a difference between the modeled lidar ratios is mainly due to overestimated concentration at the large particle end by the retrieval algorithm. In the dust layer, however, the coarse mode is a significant contributor to both extinction and backscattering coefficients (Figure 3), so that an increase in backscattering is largely compensated by an increase in extinction, when calculating the lidar ratio.

5. COMPARISON OF THE MODELED LIDAR RATIO WITH THAT DERIVED FROM THE LIDAR/SUNPHOTOMETER MEASUREMENTS

The vertically resolved lidar ratio implied by the extinction profile (Schmid et al. 2003) is also shown in Figure 1, for comparison with the modeled values. The uncertainties in the implied lidar ratio were estimated considering the following sources of error: sunphotometer-derived extinction data and aerosol optical depth data up to each altitude; normalized relative backscatter; and the lidar constant needed to interpret the lidar data. As mentioned before, the modeled lidar ratio is highly sensitive to aerosol properties assumed in the model. Thus, comparison between the modeled lidar ratio and that derived from sunphotometer/lidar measurements is useful to test the validity of the model.

Uncertainties in the modeled lidar ratios are summarized in Table 3. As already noted, there was no information on vertical variability of the refractive indices within the studied layers. Sensitivity of the modeled lidar ratio to variations in the real part of the refractive index was therefore examined by varying this parameter by $\pm 5\%$. In order to estimate the uncertainty in the modeled lidar ratio due to the uncertainty in the imaginary part of refractive index, we were guided by single scattering albedo values (indicated in Table 3) derived from in-situ measurements (Anderson et al. 2003; Markowicz et al. 2003; Carrico et al. 2003; Quinn et al. 2004), and Spectral Solar Flux Radiometer (SSFR) measurements (Bergstrom et al. 2003). For that purpose the imaginary part of refractive index was varied by a constant percentage through the entire particle size range, to obtain the desired single scattering albedo value.

We also examined the effect of variations of RH around the average values for the layers studied (55%, 63%, and 49% in the boundary, pollution and dust layers, respectively) on the

TABLE 3
Uncertainties in calculated lidar ratios in three observed layers in the aerosol profile observed on April 17, 2001

	Retrieved size distributions			Measured size distributions		
Sources of errors	Boundary layer	Pollution layer	Dust layer	Boundary layer	Pollution layer	Dust layer
Aerosol size distribution	(−15.2%, +0.7%)	(−15.2%, +0.7%)	(−15.2%, +0.7%)	(−13.6%, +15.9%)	(−11.0%, +12.4%)	(−6.2%, +11.2%)
Refractive index (real part) ±5%	(−46.0%, +53.0%)	(−15.1%, +28.2%)	(−45.9%, +107.8%)	(−41.6%, +49.2%)	(−25.8%, +24.3%)	(−42.0%, +109.9%)
Refractive index (imaginary part)*	(+12.5%, +84.7%)	(−24.2%, −38.5%)	(−5.1%, +11.2%)	(+12.1%, +88.1%)	(−29.1%, −45.5%,)	(−5.1%, +11.2%)

*The imaginary part of the refractive index was varied to yield the following single scattering albedo values: 0.88–0.98 in the boundary layer, 0.88–0.94 in the pollution layer and 0.92–0.96 in the dust layer.

modeled lidar ratio. Since the size distributions used in the model were adjusted to ambient RH, the variations in RH would affect the modeled optical properties through variations in the refractive index values used in the model. Using the information on chemical compositions of fine and coarse particle modes in different layers (given by Wang et al. 2002) and refractive index values of various aerosol components at a range of RH values from the OPAC database (Hess et al. 1998), we estimated the effect of the variations on modeled lidar ratio. An increase in RH leads to a decrease in both the real and imaginary parts of the refractive index. These changes have the opposite effects on the calculated lidar ratio: a decrease in the real part leads to an increase in lidar ratio, while a decrease in the imaginary part leads to a decrease in lidar ratio. The estimated effect of RH variation on modeled lidar ratio is therefore not large in the pollution and dust layers: the resulting lidar ratio variations are 1.5–3.0 sr and ∼1.0 sr in these layers, respectively. The effect in the boundary layer is larger (about 50%) at altitudes between ∼0.15 and 0.25 km, due to significant deviation of the RH from the average value for this layer, and lack of absorption. In the remaining part of this layer, the effect is similar to that in the pollution and dust layers.

The error bars in the lidar ratios modeled from the measured size distributions, shown in Figure 1 for better understanding of the comparison between the modeled and implied lidar ratios, are due to uncertainties in the size distributions (Wang et al. 2002) and the real part of the refractive index. In Figure 1 we also indicate a range of lidar ratio values calculated using imaginary parts of refractive indices which yield single scattering albedos in agreement with the measurements, for each size distribution model. In the case of the boundary layer, we extend the range of single scattering albedo values to 0.88 (the lower value for the pollution layer), as no clear boundary between these two layers is observed in the extinction profile. In the following text, we discuss these comparisons in each layer separately.

Marine Boundary Layer

The implied lidar ratio has large values in the boundary layer (larger than 50 sr in a significant part of the layer), whereas the modeled values (using the measured size distributions and those retrieved from sunphotometer-derived extinction spectra) in this layer are generally smaller than the lidar ratios of maritime aerosol reported in the literature. Cattrall et al. (2005) obtained a value of 28 ± 5 sr at 0.55 μm for maritime aerosol, from calculations based on over a thousand retrievals of aerosol properties from selected AERONET (Holben et al. 1998) sites. Masonis et al. (2003) reported a value of 25.4 ± 3.5 sr at 0.532 μm, obtained from measurements using an integrating nephelometer, a Particle Soot Absorption Photometer (PSAP), and a 180°-backscatter nephelometer, under clean marine conditions, for near-ambient RH. Using MPL/sunphotometer measurements during the INDOEX campaign, Welton et al. (2002) obtained a value of 33 ± 6 sr for marine aerosols without continental influence. Horizontal inhomogeneity of the layer, reported by Wang et al. (2002), is a possible cause of low modeled lidar ratio values in the present study. As mentioned earlier, it affects the sunphotometer-derived extinctions, thus affecting both the implied lidar ratio and the lidar ratio modeled using the size distributions retrieved from the extinction spectra.

For another aerosol profile studied by Schmid et al. (2003) (observed on April 6, 2001, at a location close to the location of the measurements studied here), the implied lidar ratio obtained following the same procedure exhibits lidar ratio values of 25–35 sr, typical for maritime aerosol, thus excluding the possibility of the inaccurate correction for the overlap effect (an incomplete overlap between the laser beam and the receiver field of view (Welton et al. 2002). This layer was more homogeneous. The corresponding sunphotometer-derived extinction spectra display larger wavelength dependence than in the case studied here (April 17), suggesting a larger relative contribution of small particles. It should be noted that the wavelength dependence of sunphotometer-derived aerosol extinction did not show significant change with altitude. We computed the lidar ratio values using aerosol size distributions retrieved from extinction spectra derived for this profile, and the refractive index for the marine boundary layer in the profile of April 17. The calculated lidar ratio for low altitudes (below ∼0.25 km) was between 22 and 25 sr, in agreement with the implied lidar ratio values at these altitudes. However, the implied lidar ratio increased with altitude above ∼0.25 km, while the modeled lidar ratio did not show significant change.

In this study, the refractive index model used for the marine boundary layer in the April 17 case could be representative at low altitudes, while not applicable at higher altitudes. It is likely that particles at higher altitudes in the boundary layer studied here are absorbing (note that there is no clear boundary between the marine boundary and pollution layer). Lidar ratio profiles corresponding to single scattering albedo values of 0.98 and 0.88 (Figure 1) show that a significant increase in lidar ratio can be realized by substantially increasing aerosol absorption. We conclude that the most probable reasons for the low modeled lidar ratio values in the present work are uncertainties in sunphotometer-derived extinction spectra caused by layer inhomogeneity, and lack of information on the vertical variability of particle refractive index.

Pollution Layer

In the pollution layer, the lidar ratio values calculated from the retrieved size distributions are closer to the implied values than those calculated from the measured particle size distributions. However, in the case of the latter size distribution model, combined uncertainties in size distributions and real part of refractive index can explain these larger differences. The differences between the lidar ratios resulting from the retrieved size distributions, and the implied lidar ratios at different altitudes in this layer, range from 7% to 46%. Note that we do not consider the part of the pollution layer above 1.9 km, due to unrealistically large implied lidar ratio. These differences are within the uncertainties of the implied lidar ratios at most altitudes. However, the modeled lidar ratios systematically overestimate the implied

lidar ratio in this layer. Analysis of the effect of the assumption of internally mixed sea salt and dust in the coarse mode particles revealed that it results in an overestimated lidar ratio modeled using the retrieved size distributions by 15–32%. A smaller effect was obtained at lower altitudes, where the fine mode dominated the particle size distribution. In the case of lidar ratio calculated from the measured size distributions, the overestimation was higher (32–44%). The assumption of an external mixture led to closer agreement between the results of the two size distribution models, and a very good agreement between the modeled and implied lidar ratios. We also examined other sources of uncertainties in the modeled lidar ratio. The modeled lidar ratio profiles for the cases with single scattering albedo values of 0.88 and 0.94 (Figure 1) show that uncertainty in the imaginary part of the refractive index is significant enough to explain the differences between the modeled and the implied lidar ratios.

As noted before, the size distributions retrieved from the spectral dependence of aerosol optical properties are not unique. Since our analysis showed that the size distribution retrieved using the constrained linear inversion method overestimates the lidar ratio (Table 3), it is of interest to compare this size distribution with the range of distributions derived from combined lidar measurements and the same extinction spectra. Therefore, an attempt was made here to find the range of the bimodal lognormal size distributions equivalent to those retrieved using the constrained linear inversion method (in the sense that they reproduce the measured extinction spectra), which also reproduce the implied lidar ratio values within the estimated uncertainties. For this purpose, a look-up-table (LUT) approach was used. In order to generate the look-up-table, the aerosol optical properties (extinction and scattering coefficients, and phase function in the backward direction) were calculated for a range of lognormal functions, using the same size-resolved refractive index which was used in the previous calculations. The bimodal lognormal size distribution function is defined as:

$$n(r) = \sum_{i=1}^{2} \frac{N_{0i}}{\sqrt{2\pi}\sigma_i} \exp\left(-\frac{(\ln r - \ln r_{mi})^2}{2\sigma_i^2}\right) \qquad [4]$$

where N_{0i} is the total particle concentration, and r_{mi} and σ_i are the mode radius and width of the ith mode. The modal radius of the accumulation mode was varied between 0.04 μm and 0.20 μm, in steps of 0.02 μm, while the modal radii of the coarse mode were chosen in the range 0.25 to 1.30 μm, with increments of 0.05 μm. The respective widths were varied in the range 0.40–0.70 and 0.40–0.90, for the accumulation and coarse mode, in steps of 0.05. While this range of parameters for the accumulation mode is made to include the values resulting from size distribution retrievals using the non-linear least squares method in Part I, in the case of the coarse mode, larger values had to be considered in order to enhance the backscattering coefficient. The fine and coarse lognormal modes were then combined in order to find the size distributions such that the calculated optical properties agree with the sunphotometer measurements and the implied lidar ratio within the uncertainties. For all combinations of fine and coarse modes from the look-up-table, the following quantities were calculated:

$$\varepsilon_{\text{ext}} = \sqrt{\frac{1}{13}\sum_{i=1}^{13}\left(\frac{\sigma_{\text{ext}}^{\text{meas}}(\lambda) - \sigma_{\text{ext}}^{\text{calc}}(\lambda)}{\sigma_{\text{ext}}^{\text{meas}}(\lambda)}\right)^2} \qquad [5]$$

and

$$\Delta_S = \frac{\left|S^{\text{implied}} - S^{\text{calc}}\right|}{S^{\text{implied}}} \qquad [6]$$

Here, $\sigma_{\text{ext,}}^{\text{meas}}(\lambda)$ and $\sigma_{\text{ext,}}^{\text{calc}}(\lambda)$ are measured and calculated aerosol extinction coefficients at wavelength λ, while S_{implied} and S_{calc} are the implied and calculated lidar ratios.

For this analysis, we used sunphotometer-derived extinction spectra and implied lidar ratios at lower altitudes in the pollution layer, where the effect of the assumption of an internal mixture of sea salt and dust is less significant (because of the dominant fine particle mode). By requiring that the retrieved size distributions yield aerosol extinction and lidar ratios in agreement with sunphotometer and lidar measurements within given

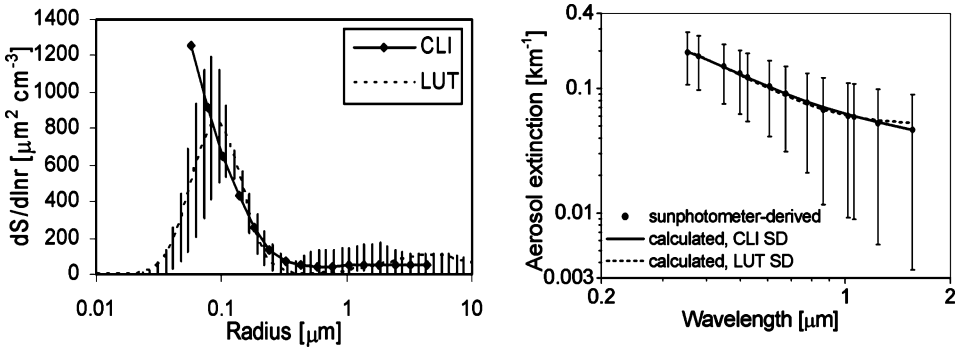

FIG. 4. Comparison of size distributions, derived using LUT and constrained linear inversion methods from the sunphotometer-derived extinction and corresponding extinction spectra at the altitude $h = 0.63$ km.

uncertainties, multiple solutions were obtained. However, in all cases, the solutions were grouped around a single combination of parameter values. The final solution was found from minimizing the sum of squares of the two residual quantities defined by Equations (5) and (6). These size distributions exhibit a wide coarse mode, since the larger particles need to be included to increase the backscattering, and consequently decrease the lidar ratio. At all altitudes considered, the smaller lidar ratio produced by the LUT-derived size distributions is achieved by large values of the coarse mode radius and width. A typical case is shown in Figure 4, for the altitude h = 0.63 km, where the largest difference (46%) between the implied lidar ratio, and the one modeled (using the size-resolved refractive index model (Wang et al. 2002)) by the size distribution retrieved using the constrained linear inversion method, was obtained. The LUT-derived size distribution yields slightly smaller extinction and 41% larger backscattering at $\lambda = 0.523$ μm than the size distribution retrieved using the constrained linear inversion method. Figure 4 also shows the extinction spectrum predicted by the LUT-derived size distribution, in comparison with that derived from the sunphotometer measurements. The difference at the largest wavelength is within the estimated uncertainties of the sunphotometer-derived extinction. This example shows that, in aerosol models based on size distributions retrieved from extinction spectra using the constrained linear inversion method, lack of information beyond the radius limits of the retrieval can cause large uncertainties in the modeled backscattering, even in the case of a dominant fine particle mode.

Dust Layer

As noted previously, in the dust layer, the use of Mie theory for calculating lidar ratio is a major reason for obtaining low values in the range between 9.1 sr and 13.1 sr, significanly lower than the implied lidar ratio (29–47 sr in the central part of the layer, in which the extinction is larger), and also lower than the directly measured lidar ratio values for Asian dust reported in other studies. Sakai et al. (2002) reported an average lidar ratio value of 46 $\pm$ 5 sr obtained by Raman lidar measurements at 0.532 μm, for an elevated dust layer over Tsukuba, on April 23. Studying Asian dust events in 1998 and 1999, using a high spectral resolution lidar and a combined Raman elastic-backscatter lidar, Liu et al. (2002) reported height-averaged values of 42–55 sr at two sites in Japan. In most of the central part of the layer, the uncertainties due to size distribution and refractive index (both the real and imaginary parts) only partly explain the differences between the modeled and implied lidar ratios. Small variations in retrieved size distributions (constrained by the uncertainties in measured extinction coefficients) result in small changes in calculated lidar ratio (by 1–2 sr).

It is likely that particle nonsphericity is responsible for lower modeled lidar ratio. Mishchenko et al. (1997) suggested a model of randomly oriented oblate and prolate spheroids, with a wide range of shapes, for calculation of optical properties of nonspherical dust particles. Using the T-matrix algorithm (Mishchenko and Travis 1998), they reported that Mie theory underestimated lidar ratio by a factor of 1.5–3.0 (depending on particle size distribution), compared to the spheroidal model. Mattis et al. (2002) carried out a comparison of modeled lidar ratio (using Mie theory) with lidar measurements, and reported that the correction suggested by Mishchenko et al. (1997) yielded agreement between the model and the measurements. Following these studies, assuming that particle nonsphericity is responsible for the larger lidar ratio values obtained from the measurements, we applied the correction factor of 3.0 to modeled lidar ratios in the central part of the dust layer (between 2.5 and 3 km) studied in the present work, to obtain lidar ratio values for a mixture of oblate and prolate surface-equivalent spheroids. We obtained the layer-averaged values of 35.7 sr and 31.2 sr, in agreement with the implied lidar ratio values (Figure 1).

6. CONCLUSION

Comparison between the modeled lidar ratio and that derived from co-located airborne sunphotometer and shipborne lidar measurements (the "implied" lidar ratio calculated by Schmid et al. 2003) was carried out for a vertical profile with three distinct aerosol layers, observed during the ACE-Asia campaign on April 17. For that purpose, size distributions retrieved from sunphotometer-derived extinction spectra, and those measured in-situ using a combination of DMA and APS flown on the same aircraft as the sunphotometer, were combined with the same size-dependent refractive indices calculated for each layer by Wang et al. (2002) on the basis of particle chemical composition analysis. The calculated single scattering albedos did not show significant vertical variability within the layers, and the values of 0.78–0.81 and 0.93–0.96 (at $\lambda = 0.523$ μm) in the pollution and dust layers, respectively, were obtained from both size distribution profiles. In the case of the dust layer, the modeled values are consistent with the in-situ measurements (Anderson et al. 2002; Markowicz et al. 2003; Carrico et al. 2003; Quinn et al. 2004), whereas in the pollution layer our model implies significantly more absorbing aerosol than obtained from the measurements. This is possibly due to uncertainties in EC refractive index used in the refractive index model, or a result of reported layer inhomogeneity and therefore non-applicability of one refractive index model to all altitudes within the layer.

Our analysis showed that an aerosol model based on size distributions retrieved from extinction spectra tends to overestimate the lidar ratio (on average by 15%), as a result of a limited radius range of retrieval. However, except for the dust layer, the retrieved size distribution led to a generally smaller lidar ratio than that derived from the measured size distributions, mainly due to their higher concentration at the small and large particle ends of the retrieved distributions. In the pollution layer, vertical profiles of modeled lidar ratios displayed an agreement with the implied lidar ratio within the estimated uncertainties. The lidar ratios derived using the retrieved size distributions yielded closer agreement with the implied lidar ratio than the lidar ratios derived using the measured in-situ size

distributions, with relative differences ranging from 7–46%. A very good agreement between he lidar ratios resulting from the two size distribution models and the implied lidar ratio in this layer was obtained assuming that the coarse mode particles were external mixtures of sea salt and dust (instead of internal mixtures, assumed in the size-resolved refractive index model by Wang et al. 2002). The assumption of an external mixture leads to significantly lower modeled lidar ratio, while having negligible effect on modeled single scattering albedo. This result shows that results of comparison between the lidar and sunphotometer measurements, using an approach which involves size distribution retrieval, strongly depend on the choice of aerosol refractive index model.

Modeled lidar ratio values in the dust layer (using Mie theory) are low compared to the implied lidar ratio. In a large part of the layer, uncertainties in aerosol size distributions and refractive indices only partly explain these differences, suggesting that particle nonsphericity is largely responsible for the lower modeled lidar ratio.

REFERENCES

Anderson L. T., Masonis, S. J., Covert, D. S., Ahlquist, N. C., Howell, S. G., Clarke, A. D., and McNaughton, C. S. (2003). Variability of Aerosol Optical Properties Derived from In Situ Aircraft Measurements During ACE-Asia, *J. Geophys. Res.* 108 (D23): 8647, doi:10.1029/2002JD003247.

Ansmann, A., Riebesell, M., and Weitkamp, C. (1990). Measurement of Atmospheric Aerosol Extinction Profiles with a Raman Lidar, *Opt. Lett.* 15:746–748.

Ansmann, A., Riebesell, M., Wandinger, U., Wietkamp, C., Voss, E., Lahmann, W., and Michealis, W. (1992). Combined Raman Elastic-Backscatter Lidar for Vertical Profiling of Moisture, Aerosol Extinction, Backscatter, and Lidar Ratio, *Appl. Phys. B* 55:18–28.

Ansmann, A., Wandinger, U., Wiedensohler, A., and Leiterer, U. (2002). Lindenberg Aerosol Characterization Experiment 1998 (LACE 98): Overview, *J. Geophys. Res.* 107 (D21), 8129, doi:10.1029/2000JD000233.

Bane, J. M., Bluth, R., Flagg, C., Jonsson, H., Melville, W. K., Prince, M., and Riemer, D. (2004). UNOLS now Oversees Research Aircraft Facilities for Ocean Science, *Eos Trans. AGU*, 85(41):402.

Bates T. S., Huebert, B. J., Gras, J. L., Griffiths, F. B., and Durkee, P. A. (1998). International Global Atmospheric Chemistry (IGAC) Project's First Aerosol Characterization Experiment (ACE 1): Overview, *J. Geophys. Res.* 103(D13):16,297–16,318.

Bergstrom, R. W., Pilewskie, P., Pommier, J., Rabbette, M., Russell, P. B., Schmid, B., Redemann, J., Higurashi, A., Nakajima, T., and Quinn, P. K. (2003). Spectral Absorption of Solarradiation by Aerosols During ACE-Asia, *J. Geophys. Res.* 109, D19S15, doi:10.1029/2003JD004467.

Bruggeman, D. (1935). Berechnung Verschiedener Physikalischer Konstanten Von Heterogenen Substanzen. I. Dielektrizit¨ Atskonstanten Und Leitf¨ Ahigkeiten Der Mischk¨ Orper Aus Isotropen Substanzen, *Ann. Phys. (Leipzig)* 24:636–679.

Carrico, C. M., Kus, P., Rood, M. J., Quinn, P. K., and Bates, T. S. (2003). Mixtures of Pollution, Dust, Sea Salt, and Volcanic Aerosol During ACE-Asia: Radiative Properties as a Function of Relative Humidity, *J. Geophys. Res.* 108 (D23), 8650, doi:10.1029/2003JD003405.

Cattrall C., Reagan, J., Thome, K., and Dubovik, O. (2005). Variability of Aerosol and Spectral Lidar and Backscatter and Extinction Ratios of Key Aerosol Types Derived from Selected Aerosol Robotic Network locations, *J. Geophys. Res.* 110, D10S11, doi:10.1029/2004JD005124.

De Rooij, W. A., and Van der Stap, C. C. A. H. (1984). Expansion of Mie Scattering Matrices in Generalized Spherical Functions, *Astronomy and Astrophysics* 131:237–248.

Ferrare, R. A., Melfi, S. H., Whiteman, D. N., Evans, K. D., Poellot, M., and Kaufman, Y. J. (1998). Raman Lidar Measurements of Aerosol Extinction and Backscattering 2. Derivation of Aerosol Real Refractive Index, Single-Scattering Albedo, and Humidification Factor Using Raman Lidar and Aircraft Size Distribution Measurements, *J. Geophys. Res.* 103 (D16):19,673–19,689.

Fiebig, M., Petzold, A., Wandinger, U., Wendisch, M., Kiemle, C., Stifter, A., Ebert, M., Rother, T., and Leiterer, U. (2002). Optical Closure for an Aerosol Column: Method, Accuracy, and Inferable Properties Applied to a Biomass-Burning Aerosol and its Radiative Forcing, *J. Geophys. Res.* 107 (D21), 8130, doi:10.1029/2000JD000192.

Gonzalez Jorge, H., and Ogren, J. A. (1996). Sensitivity of Retrieved Aerosol Properties to Assumptions in the Inversion of Spectral Optical Depths, *J. Atmos. Sci.* 53:3669–3683.

Grund, C. J., and Eloranta, E. W. (1990). The 27–28 October 1986 FIRE Cirrus Case Study: Cloud Optical Properties Determined by High Spectral Resolution Lidar, *Mon. Wea. Rev.* 118.

Hess, M., Koepke, P., and Schult, I. (1998). Optical Properties of Aerosols and Clouds: The Software Package OPAC, *Bull. Am. Meteor. Soc.* 79:831–844.

Holben, B. N., Eck, T. F., Slutsker, I., Tanre, D., Buis, J. P., Setzer, A., Vermote, E., Reagan, J. A., Kaufman, Y., Nakajima, T., Lavenu, F., Jankowiak, I., and Smirnov, A. (1998). AERONET: A Federated Instrument Network and Data Archive for Aerosol Characterization, *Remote Sens. Environ.* 66:1–16.

Huebert, B. J., Bates, T., Russell, P. B., Shi, G., Kim, Y. J., Kawamura, K., Carmichael, G., and Nakajima, T. (2003). An Overview of ACE-Asia: Strategies for Quantifying the Relationships Between Asian Aerosols and Their Climatic Impacts, *J. Geophys. Res.* 108(D23), 8633, doi:10.1029/2003JD003550.

IPCC. (2001). *Climate Change 2001: The Scientific Basis. Contribution of Working Group I to the Third Assessment Report of the Intergovernmental Panel on Climate Change* (Houghton, J. T., Ding, Y., Griggs, D. J., Noguer, M., van der Linden, P. J., Dai, X., Maskell, K., and Johnson, C. A. (eds.)). Cambridge University Press, Cambridge, United Kingdom and New York, NY, USA, p. 881.

Kalashnikova, O., and Sokolik, I. N. (2002). Importance of Shapes and Composition of Wind-Blown Dust Particles for Remote Sensing at Solar Wavelengths, *Geophys. Res. Lett.* 29, No.10, 10.1029/2002GL014947.

Kalashnikova, O. V., and Sokolik, I. N. (2004). Modeling the Radiative Properties of Nonspherical Soil-Derived Mineral Aerosols, *JQSRT* 87:137–166.

King, M. D., Byrne, D. M., Herman, B. M., and Reagan, J. A. (1978). Aerosol Size Distributions Obtained by Inversion of Spectral Optical Depth Measurements, *J. Atmos. Sci.* 35:2153–2167.

King, M. D. (1982). Sensitivity of Constrained Linear Inversions to the Selection of the Lagarange Multiplier, *J. Atmos. Sci.* 39:1356–1369.

Kuzmanoski, M., Box, M. A., Box, G. P., Schmid, B., Wang, J., Russell, P. B., Jonsson, H. H., and Seinfeld, J. H. (2006). Aerosol Properties Computed from Aircraft-based Observations During the ACE-Asia Campaign: 1. Aerosol Size Distributions Retrieved from Optical Thickness Measurements, *Aerosol Science and Technology* (in press).

Liu, Z., Sugimoto, N., and Murayama, T. (2002). Extinction-to-Backscatter Ratio of Asian Dust Observed with High-Spectral-Resolution Lidar and Raman lidar, *Appl. Opt.* 41**:**2760–2767.

Markowicz, K. M., Flatau, P. J., Quinn, P. K., Carrico, C. M., Flatau, M. K., Vogelmann, A. M., Bates, D., Liu, M., and Rood, M. J. (2003). Influence of Relative Humidity on Aerosol Radiative Forcing: An ACE-Asia Experiment Perspective, *J. Geophys. Res.* 108(D23)**,** 8662, doi:1029/2002JD003066.

Masonis, S. J., Anderson, T. L., Covert, D. S., Kapustin, V., Clarke, A. D., Howell, S., and Moore, K. (2003). A study of the extinction-to-backscatter ratio of marine aerosol during the Shoreline Environment Aerosol Study, *J. Atmos. Oceanic Technol.* 20:1388–1402.

Mattis, I., Ansmann, A., Muller, D., Wandinger, U., and Althausen, D. (2002). Dual-Wavelength Raman Lidar Observations of the Extinction-to-Backscatter Ratio of Saharan Dust, *Geophys. Res. Lett.* 29, 1306, doi:10.1029/2002GL014721.

McGill, M. J., Hlavka, D. L., Hart, W. D., Welton, E. J., and Campbell, J. R. (2003). Airborne Lidar Measurements of Aerosol Optical Properties During SAFARI-2000, *J. Geophys. Res.* 108, doi:10.1029/2002JD002370.

Mishchenko, M. I., Travis, L. D., Kahn, R. A., and West, R. A. (1997). Modeling Phase Functions for Dustlike Tropospheric Aerosols Using a Shape Mixture of Randomly Oriented Polydisperse Spheroids, *J. Geophys. Res.* 102:16,831–16,847.

Mishchenko, M. I., and Travis, L. D. (1998). Capabilities and Limitations of a Current FORTRAN Implementation of the T-Matrix Method for Randomly Oriented, Rotationally Symmetric Scatterers, *J. Quant. Spectrosc. Radiat. Transfer* 60:309–324.

Mishchenko, M. I., Dlugach, J. M., Yanovitskij, E. G., and Zakharova, N. T. (1999) Bidirectional Reflectance of Flat, Optically Thick Particulate Layers: An Efficient Radiative Transfer Solution and Applications to Snow and Soil Surfaces, *J. Quant. Spectrosc. Radiat. Transfer* 63:409–432.

Nenes, A., Pandis, S., and Pilinis, C. (1998). ISORROPIA: A New Thermodynamic Equilibrium Model for Multiphase Multicomponent Inorganic Aerosols, *Aquat. Geochem.* 4:123–152.

Pilinis C., and Li, X. (1998). Particle Shape and Internal Inhomogeneity Effect on the Optical Properties of Tropospheric Aerosols of Relevance to Climate Forcing, *J. Geophys. Res.* 103:3789–3800.

Powell, D. M., Reagan, J. A., Rubio, M. A., Erxleben, W. H., and Spinhirne, J. D. (2000). ACE-2 Multiple Angle Micro-Pulse Lidar Observations from Las Galletas, Tenerife, Canary Islands, *Tellus* 52B:652–661.

Quinn, P. K., Coffman, D. J., Bates, T. S., Welton, E. J., Covert, D. S., Miller, T. L., Johnson, J. E., Maria, S., Russell, L., Arimoto, R., Carrico, C. M., Rood, M. J., and Anderson, J. (2004). Aerosol Optical Properties Measured on Board the *Ronald H. Brown* During ACE-Asia as a Function of Aerosol Chemical Composition and Source Region, *J. Geophys. Res.* 109, D19S01, doi:10.1029/2003JD004010.

Rajeev, K., and Parameswaran, K. (1998). Iterative Method for the Inversion of Multiwavelength Lidar Signals to Determine Aerosol Size Distribution, *Appl. Opt.* 37:4690–4700.

Reagan, J. A., Apte, M. V., Ben-David, A., and Herman, B. M. (1988). Assessment of Aerosol Extinction to Backscatter Ratio Measurements made at 694.3 nm in Tucson, Arizona, *Aerosol Science and Technology* 8:215–226.

Redemann J., Turco, R. P., Pueschel, R. F., Fenn, M. A., Browell, E. V., and Grant, W. B. (1998). A Multi-Instrument Approach for Characterizing the Vertical Structure of Aerosol Properties: Case Studies in the Pacific Basin Troposphere, *J. Geophys. Res.* 103:23,287–23,298.

Redemann, J., Turco, R. P., Liou, K. N., Russell, P. B., Bergstrom, R. W., Schmid, B., Livingston, J. M., Hobbs, P. V., Hartley, W. S., Ismail, S., Ferrare, R. A., and Browell, E. V. (2000). Retrieving the Vertical Structure of the Effective Aerosol Complex Index of Refraction from a Combination of Aerosol in Situ and Remote Sensing Measurements During TARFOX, *J. Geophys. Res.* 105 (D8):9949–9970.

Russell, P. B., Swissler, T. J., McCormick, M. P., Chu, W. P., Livingston, J. M., and Pepin, T. J. (1981). Satellite and Correlative Measurements of the Stratospheric Aerosol. I: An Optical Model for Data Conversions, *J. Atmos. Sci.* 38:1279–1294.

Russell, P. B., Hobbs, P. V., and Stowe, L. L. (1999). Aerosol Properties and Radiative Effects in the United States East Coast Haze Plume: An Overview of the Tropospheric Aerosol Radiative Forcing Observational Experiment (TARFOX), *J. Geophys. Res.*, 104:2213–2222.

Russell, P. B., and Heintzenberg, J. (2000). An Overview of the ACE-2 Clear Sky Column Closure Experiment (CLEARCOLUMN), *Tellus* 52B:463–483.

Sakai, T., Shibata, T., Iwasaka, Y., Nagai, T., Nakazato, M., Matsumura, T., Ichiki, A., Kim, Y-S, Tmura, K., Troshkin, D., Hamdi, S. (2002). Case Study of Raman Lidar Measurements of Asian Dust Events in 2000 and 2001 at Nagoya and Tsukuba, Japan, *Atmos. Environ.* 36: 5479–5489.

Schmid, B., Hegg, D. A., Wang, J., Bates, D., Redemann, J., Russell, P. B., Livingston, J. M., Jonsson, H. H., Welton, E. J., Seinfeld, J. H., Flagan, R. C., Covert, D. S., Dubovik, O., and Jefferson, A. (2003). Column Closure Studies of Lower Tropospheric Aerosol and Water Vapor During ACE-Asia Using Airborne Sun Photometer and Airborne in Situ and Ship-Based Lidar Measurements, *J. Geophys. Res.* 108 (D23), 8656, doi:10.1029/2002JD003361.

Shipley, S. T., Tracy, D. H., Eloranta, E. W., Trauger, J. T., Sroga, J. T., Roesler, F. L., and Wienman, J. A. (1983). High Spectral Resolution Lidar to Measure Optical Scattering Properties of Atmospheric Aerosols. 1. Theory and Instrumentation, *Appl. Opt.* 22:3716–3724.

Sokolik I. N., Winker, D. M., Bergametti, G., Gillette, D. A., Carmichael, G., Kaufman, Y. J., Gomes, L., Schuetz, L., and Penner, J. E. (2001). Introduction to Special Section: Outstanding Problems in Quantifying the Radiative Impacts of Mineral Dust, *J. Geophys. Res.* 106 (D16):18,015–18,027.

Spinhirne, J. D., Reagan, J. A., and Herman, B. M. (1980). Vertical Distribution of Aerosol Extinction Cross Section and Inference of Aerosol Imaginary Index in the Troposphere by Lidar Technique, *J. Appl. Meteorol.* 19:426–438.

Spinhirne, J. D., Rall, J. A. R., and Scott, V. S. (1995). Compact Eye Safe Lidar Systems, *Rev. Laser. Eng.* 23:112–118.

Wang, J., Flagan, R. C., Seinfeld, J. H., Jonsson, H. H., Collins, D. R., Russell, P. B., Schmid, B., Redemann, J., Livingston, J. M., Gao, S., Hegg, D. A., Wetton, E. J., and Bates, D. (2002). Clear-Column Radiative Closure During ACE-Asia: Comparison of Multiwavelength Extinction Derived from Particle Size and Composition with Results from Sun Photometry, *J. Geophys. Res*, 107(D23), 4688, doi:10.1029/2002JD002465.

Welton, E. J., Voss, K. J., Gordon, H. R., Maring, H., Smirnov, A., Holben, B., and Schmid, B., Livingston, J. M., Russell, P. B., Durkee, P. A., Formenti, P., Andreae, M. O. (2000). Ground-Based Lidar Measurements of Aerosols During ACE-2: Instrument Description, Results, and Comparisons with other Ground-Based and Airborne Measurements, *Tellus*, 52B:636–651.

Welton, E. J., Campbell, J. R., Spinhirne, J. D., and Scott, V. S. (2001). *Global Monitoring of Clouds and Aerosols Using a Network of Micro-Pulse Lidar Systems*, in Lidar Remote Sensing for Industry and Environmental Monitoring, edited by U. N.

Welton, E. J., Voss, K. J., Quinn, P. K., Flatau, P. J., Markowicz, K., Campbell, J. R., Spinhirne, J. D., Gordon, H. R., and Johnson, J. E. (2002). Measurements of Aerosol Vertical Profiles and Optical Properties During INDOEX 1999 Using Micropulse Lidars, *J. Geophys. Res.* 107(D19), 8019, doi:10.1029/2000JD000038.